
ELSEVIER

Nuclear Instruments and Methods in Physics Research B 142 (1998) 441–462

NIM B
Beam Interactions with Materials & Atoms

Charge states of relativistic heavy ions in matter

C. Scheidenberger [a,*], Th. Stöhlker [a], W.E. Meyerhof [b], H. Geissel [a], P.H. Mokler [a], B. Blank [c]

[a] *Gesellschaft für Schwerionenforschung, Planckstrasse 1, 64291 Darmstadt, Germany*
[b] *Department of Physics, Stanford University, CA 94305, USA*
[c] *Centre d'Études Nucléaires de Bordeaux, 33175 Gradignan, France*

Received 5 January 1998

Abstract

Experimental and theoretical results on charge-exchange cross-sections and charge-state distributions of relativistic heavy ions penetrating through matter are presented. The data were taken at the Lawrence Berkeley Laboratory's BEVALAC accelerator and at the heavy-ion synchrotron SIS of GSI in Darmstadt in the energy range 80–1000 MeV/u. Beams from Xe to U impinging on solid and gaseous targets between Be and U were used. Theoretical models for the charge-state evolution inside matter for a given initial charge state are presented. For this purpose, computer codes have been developed, which are briefly described. Examples are given which show the successes and limitations of the models.

1. Introduction

The advent of relativistic heavy-ion accelerators, as well as new applications with relativistic heavy-ion beams, require a detailed knowledge of atomic collision processes. For instance, accelerators need efficient strippers which induce only small emittance blow-up. High ionic charge states allow for lower power consumption and/or smaller machines, thus reducing their price and their operational costs. It is desirable to use as few stripper stations as possible in order to minimize losses of beam intensity.

For the design and operation of storage rings for heavy ions and colliders such as ESR (Darmstadt), RHIC (Brookhaven) and LHC (Geneva), one has to know precisely the interaction cross-sections with the residual gas and colliding beams in order to estimate beam lifetimes and loss rates. Also, in the multiple-turn passage through these devices, the charge-state distribution of the beam will evolve, with subsequent beam loss.

State selective atomic-collision experiments, such as radiative transfer and excitation (RTE) measurements, require known initial charge states. For the interpretation of many nuclear-physics experiments, a knowledge of ionic charge-state distributions is decisive, for instance for the determination of the nuclear-charge yields of fission products.

* Corresponding author. Tel.: +49-6159-71-2706; fax: +49-6159-71-2902; e-mail: c.scheidenberger@gsi.de.

0168-583X/98/$19.00
PII: S0168-583X(98)00244-4

Indeed, the first experimental results on ionic charge-state distributions for heavy ions were obtained with fission fragments by Lassen [1]. Interesting effects, such as the gas–solid difference in the mean charge state were discovered. However, due to the wide energy spread of fission fragments, these experiments could not be very detailed. Moreover, the huge charge-changing cross-sections at low energies and the target preparation techniques at the time, did not allow for cross-section measurements under single-collision conditions.

Pioneering theoretical work was done by Bohr [2] and Bohr and Lindhard [3]. The so-called Bohr criterion that projectile electrons are stripped off during the penetration of matter if their orbital velocity is smaller than the projectile velocity, was established and proven to be in good agreement with experimental findings. Although this criterion is very useful and can be applied successfully even at relativistic velocities, it does not incorporate any target dependence. In later years, many semi-empirical parameterizations were developed, see e.g. [4], to describe the energy and target dependence of the mean charge and the width of charge-state distributions.

Once the cross-sections are known, the charge-state evolution for ions having any initial charge state can be obtained from the solution of rate equations. For up to three charge states, they can be easily solved analytically [5]. Beyond this number of charge states, numerical approaches are used frequently. A general analytical scheme for an arbitrary number of charge states has been derived by Sigmund [6]. For heavy ions, many charge states typically contribute to the charge-state distribution. Thus, in principle, one needs to know all the relevant cross-sections for excitation, decay, ionization and capture for all contributing ground and excited states. One may overcome these difficulties, by using 'effective' cross-sections for capture and loss, derived from the measured target-thickness dependence of charge-state fractions [7]. For relativistic heavy ions, the situation generally is simplified compared to low energies, since at charge-state equilibrium even the heaviest ions carry only few electrons during their passage through matter. Fig. 1 compares equilibrium charge-state spectra of U projectiles in carbon at 1.4, 11.5 and 950 MeV/u. As depicted in this comparison, at low energies the charge-state spectrum is broad and bare ions cannot be produced whereas at high enough energies the charge-state distribution receives contributions only from bare, H- and He-like ions in charge-state equilibrium. At still higher energy, the bare-ion fraction dominates. At low energies, carbon is the best stripper whereas at high energies carbon is a poor stripper as compared to heavier target materials. The reason will be explained below.

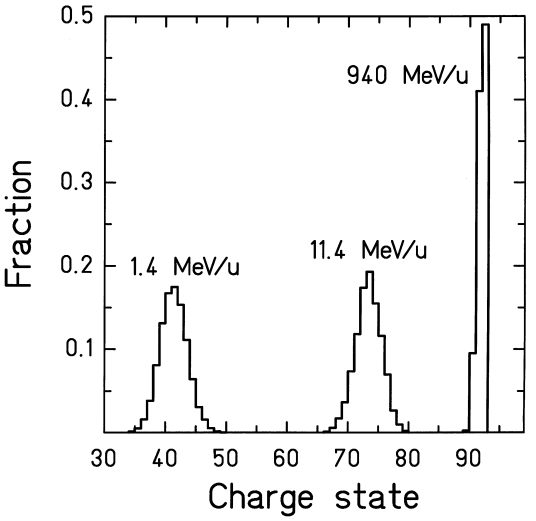

Fig. 1. Equilibrium charge-state spectra of U projectiles behind C foils: the left spectrum was measured at the UNILAC of GSI behind a 40-μg/cm^2 thick target for an entrance energy of 1.4 MeV/u [8], the distribution depicted in the middle of the figure was obtained behind a 490 μg/cm^2 target and an incident energy of 11.5 MeV/u (courtesy of B. Franzke) [9], and the spectrum displayed on the right was measured at SIS behind a 400 mg/cm^2 target at an entrance energy of 940 MeV/u.

New experimental techniques have been developed which give detailed insights into specific charge-changing processes [10]. The observation of photons emitted in radiative electron capture (REC) is possible [11] and coincidence techniques [12] allow the measurement of differential REC cross-sections. Subshell resolved excitation cross-sections also can be obtained [13,14]. A striking feature of atomic-collision experiments with relativistic heavy ions is that charge-changing cross-sections can be studied under single-collision conditions in solids. Gas-jet targets at storage

rings, such as at the ESR at GSI, open up unique new experimental opportunities in this respect.

The purpose of this paper is to summarize theoretical and experimental results on charge-changing cross-sections, charge-state evolutions, and equilibrium charge-state distributions. The data are derived from experiments carried out at the BEVALAC (Berkeley) and at the heavy-ion synchrotron SIS of GSI (Darmstadt) and associated facilities. Representative data, partly unpublished so far, are given for Xe, Au, and U projectiles impinging with kinetic energies from 80 to 1000 MeV/u on targets ranging from Be to U. For experimental details, the reader is referred to [15–25]. Phase-state, directional, and ultra-relativistic effects are beyond the scope of the present paper. Only charge states of relativistic *projectiles* are considered throughout this paper. Theoretical models and their range of applicability are discussed. The models are implemented in two computer codes developed for practical applications and able to take into account, respectively, up to three and up to 28 electrons attached to the projectile. The results are compared with experimental data.

2. Physical background

The modeling of charge-state distributions of ion beams passing through matter requires the knowledge of the basic interaction mechanisms between highly charged ions and neutral matter, i.e., the processes of projectile excitation, deexcitation, and ionization, and of electron capture into empty projectile states. The lifetimes of excited ionic states may have to be taken into account, particularly for solid targets. The high atomic density in a solid target may lead to important charge-changing effects caused by sequential collisions in the target. However, since lifetimes of excited states decrease dramatically with the increase of the nuclear charge number Z_P of the projectile (e.g. as $1/Z_P^4$ for allowed dipole transitions and $1/Z_P^{10}$ for spin-forbidden magnetic dipole transitions), these effects generally play a minor role for high-Z projectiles.

In the following, we discuss briefly the cross-sections for the basic processes on the basis of available experimental data. For clarity, we restrict the discussion to the simple cases of high-Z bare, H- and He-like projectiles. One finds that the general scaling laws of the charge-changing cross-sections for these ions explain the overall features of equilibrium charge-state distributions in the entire relativistic velocity domain, even quantitatively.

2.1. Cross-sections for ionization and excitation

As long as asymmetric collision systems are considered ($Z_T \ll Z_P$, where Z_T and Z_P denote the nuclear charge of target and the projectile, respectively), the ionization of H- and He-like high-Z projectile ions can be reasonably well described within first-order perturbation theory, such as the semiclassical approximation (SCA) or the plane-wave Born approximation (PWBA). Here, the basic assumptions are that only an electronic perturbation of the projectile *atomic* wave function is caused by the target nuclear charge and that the trajectory of projectile is not disturbed by the collision. Within the non-relativistic PWBA, the K-shell ionization cross-section σ_{ion} for a H-like projectile follows the simple scaling law:

$$\sigma_{ion.} = \sigma_0 f\left(\frac{v}{v_K}\right). \tag{1}$$

In this equation, $\sigma_0 = 4\pi a_0^2 Z_T^2/Z_P^4$, a_0 is the Bohr radius, and $f(v/v_K)$ is a slowly varying function of the projectile velocity v, which reaches a maximum near $v = v_K$, where v_K denotes the velocity of the active K-shell electron. Tabulated values of this function can be found in various publications (see, e.g., [20]). Even this non-relativistic approach describes the electron-loss data for relativistic high-Z projectiles reasonably well. This is shown in Fig. 2, where all available cross-section data for K-shell ionization of H- and He-like high-Z ions are summarized, which were measured for low-Z targets [18,22,27,28,26].

For comparison, all the data are scaled to the collision system $Xe^{53+} \rightarrow H^+$ by applying the scaling relation (1). The data cover an energy range between 80 and 1000 MeV/u and a projectile range between xenon and uranium. The data are plotted as a function of the reduced velocity $(v/v_K)^2$ and are compared with the non-relativistic PWBA

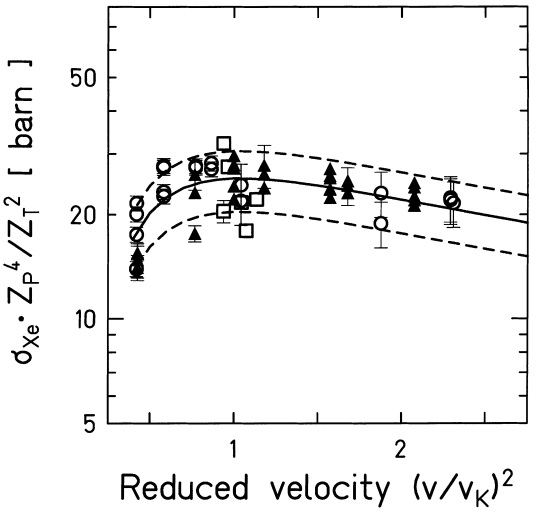

Fig. 2. Experimental ionization cross-section data per K-shell electron for H- and He-like high-Z ions impinging on low-Z targets ($Z_T < Z_P/3$). The data cover a bombarding energy range between 80 and 1000 MeV/u [26]. Open circles: results from GSI for Au and Bi projectiles in solid targets; open squares: results from GSI for Au, Pb, and U projectiles in gas targets; solid triangles: results from the BEVALAC for Xe and U projectiles in solid targets. The data, scaled to H-like Xe ions colliding with protons, are plotted as a function of the reduced velocity $(v/v_K)^2$. The solid curve gives the non-relativistic PWBA prediction and the dashed lines indicate deviations of ±20%.

predictions for $Xe^{53+} \rightarrow H^+$ collisions. Most of the data deviate by less than ±20% from Eq. (1).

To account for the relativistic effects on bound-state wave functions of high-Z projectiles, Anholt used a quasi-relativistic approximation to derive the following correction factor for the non-relativistic cross-section [29]:

$$F = \left[1 + (Z_P\alpha/2)^2\right]^{-2}, \tag{2}$$

where $\alpha \simeq 1/137$ is the fine-structure constant.

In addition, corrections due to the Lorentz transformation of the Coulombic target potential into the projectile frame must be considered, which yield the Liénard-Wiechert potential. The resulting transverse contribution to the ionization cross-section σ_{trans} is approximately given by

$$\sigma_{trans.} = \sigma_0 \frac{\ln\gamma^2 - \beta^2}{\ln(2mc^2\beta^2/E_K)}, \tag{3}$$

where $\beta = v/c$ is the projectile velocity in units of the speed of light and E_K is the K-shell binding energy of the projectile. The transverse contribution always leads to an increase of the ionization cross-section with increasing β values. The final expression for the K-shell ionization cross-section for a H-like projectile σ_K^1 is obtained from the combination of Eqs. (1)–(3) yielding

$$\sigma_K^1 = \sigma_0 F f\left(\frac{v}{v_K}\right)\left[1 + \frac{\ln\gamma^2 - \beta^2}{\ln(2mc^2\beta^2/E_K)}\right]. \tag{4}$$

The target electrons also may cause a loss of projectile electrons by impact ionization. Within first-order perturbation theory, at high collision energies this process is the same as for proton impact. Hence, the ionization by the impact of target electrons can be included approximately by substituting Z_T^2 in Eq. (1) by $Z_T^2 + Z_T$.

In Fig. 3, the relevance of the different relativistic effects for the ionization cross-sections

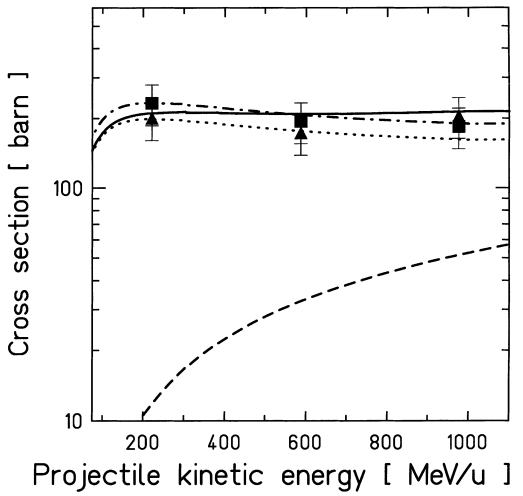

Fig. 3. Projectile ionization cross-sections for H-like Au^{78+} ions colliding with carbon (solid squares) and nickel atoms (solid up triangles) are given as a function of beam energy [22,26]. The cross sections for nickel are normalized to those for carbon (see text). The prediction of the non-relativistic PWBA approximation is represented by the dash-dotted curve and the one which includes the correction factor Eq. (2) is given by the dotted curve. The transverse ionization part, Eq. (3), is displayed separately by the dashed curve. The total ionization cross section, Eq. (4), is shown by the solid curve.

is illustrated. Projectile ionization cross-sections measured at the magnetic spectrometer FRS [22] for H-like Au^{78+} ions colliding with carbon and nickel atoms are plotted as a function of the beam energy. For presentation purposes, the cross-sections obtained for the nickel target are normalized to the ones measured for the carbon target by applying the Z_T^2 scaling law of Eq. (1). The non-relativistic PWBA calculation, which includes in addition the correction factor for the relativistic wave functions, Eq. (2), is shown by the dotted curve, whereas the result obtained from Eq. (4) is given by the solid curve. Within the considered energy regime the cross-sections vary only slightly with energy, even if the transverse ionization term is included. These findings indicate that the corrections applied here for all relativistic effects are rather small [26].

Recently, ionization cross-section data were measured for H-like Au ions at 11 GeV/u, where the transverse interaction is very pronounced [30]. Even these data are in good agreement with the above simple ionization model, where relativistic effects are considered in an approximate way. At ultra-relativistic energies screening becomes important and the experimental data obtained for 160 GeV/u Pb ions cannot be explained any longer by means of the description outlined here [31].

For more symmetric collision systems such as $Au^{78+} \rightarrow Ag$ collisions, the simple Z_T^2 scaling for projectile electron loss breaks down. Here, various effects such as multiple projectile electron loss and screening of the nuclear charge by the target electrons start to play an important role. For a detailed discussion of these effects we refer to Ref. [32]. On the other hand, for the stripper targets of most practical relevance, such as Al and Cu, the simplified treatment of the ionization process appears to be sufficient.

Excitation of projectile electrons in ion–atom collisions is mediated by the same basic mechanism as projectile ionization, except that the active electron is excited into a discrete bound state and not into a continuum of states. Similar to ionization, one may use non-relativistic first-order perturbation theory as a starting point for cross-section estimations, as done by Anholt [15] and by Anholt and Meyerhof [18]. However, already for He-like ions, the situation is rather complicated, since selection rules and the exact coupling of the electrons in each excited state must be considered [24,26]. The complexity of this process increases with the number of available projectile electrons. To date, almost no experimental data for excitation of high-Z projectiles are available [24]. With regard to charge-state distributions, excitation of projectile electrons is of importance only if the lifetimes of the excited states become comparable to the time between charge-changing collisions. Then, the effective ionization and capture cross-sections may change drastically (see Section 3.4).

2.2. Cross-sections for electron capture

Besides projectile ionization, also electron capture contributes to charge-changing channels in collisions between few-electron projectiles and neutral target atoms. The two most important processes are radiative electron capture (REC) and non-radiative electron capture (NRC).

REC dominates in high-energy collisions of high-Z projectiles with low-Z targets. Here, electron capture is accompanied by the emission of a photon. This process is the inverse of the photoelectric effect [33,34,14] and has been studied in great detail both theoretically and experimentally even for the heaviest ions up to bare uranium [35,23,14]. The non-relativistic dipole approach derived by Stobbe [33] provides a universal cross-section scaling law for the REC cross-section, valid for all non-relativistic ion–atom collision systems. The projectile atomic number Z_P and the velocity v enter the REC cross-sections through the adiabaticity parameter η, which for K-shell electrons reads

$$\eta = \frac{E_{kin}}{E_K}, \tag{5}$$

where E_{kin} is the kinetic energy of a target electron in the rest frame of the swift ion and E_K is the K-shell binding energy. An estimate for REC into the projectile K-shell REC can be obtained by using the non-relativistic dipole approach and multiplying the result with the number Z_T of quasi-free electrons in the target:

$$\sigma_{\text{K-REC}} = Z_T \cdot 9165 \quad \text{barn} \left(\frac{\kappa^3}{1+\kappa^2} \right)^2 \frac{\exp(-4\kappa \arctan \kappa^{-1})}{1-\exp(-2\pi\kappa)} \tag{6}$$

where $\kappa = 1/\sqrt{\eta}$.

Exact relativistic radiative recombination calculations by Ichihara et al. [35] demonstrate that this simple dipole approximation yields reasonable results even for high projectile charges (e.g. uranium) and relativistic beam energies up to a few hundred MeV/u. This is shown in Fig. 4, where the total electron capture cross-sections per target electron measured for bare high-Z ions (from xenon to uranium) in collisions with light target atoms are plotted versus the η-parameter [23].

The predictions of the dipole approximation are given by the dotted curve. The solid curve shows the results of the rigorous relativistic calculations performed for $Z_P = 80$ [35]. The data cover a range from $Z_P = 54$ to $Z_P = 92$ and beam energies from 80 to 1000 MeV/u. At high energies, the results of Stobbe's dipole approximation start to deviate from rigorous relativistic calculations. In this energy range, the latter can be better approximated by the Sauter formula [34], which is derived within a relativistic first-order treatment in αZ_P.

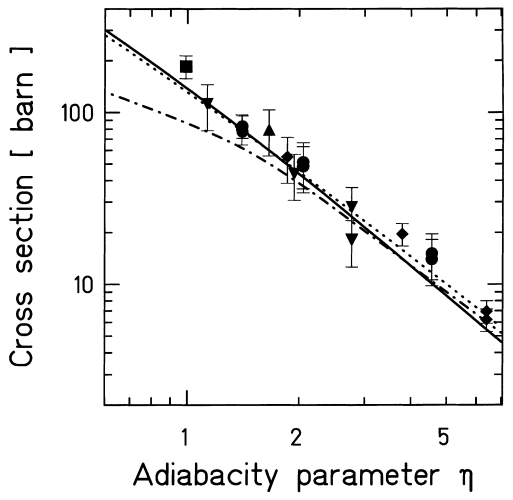

Fig. 4. K-shell REC cross sections vs. adiabaticity in comparison with experimental data (see text for details) [23]. The predictions of Stobbe's dipole approximation [33] are given by the dotted curve. The solid curve shows the results of the rigorous relativistic calculations for $Z_P = 80$ [35]. The dash-dotted curve is the (relativistic) Sauter prediction [34]. The data cover a range from $Z_P = 54$ to $Z_P = 92$ and beam energies from 80 to 1000 MeV/u.

With increasing nuclear charge of the target, the NRC process gains importance. NRC is mediated by a three-body interaction, where the third particle involved in the collision is the target atom. The active electron is transferred radiationless from a bound target state into a bound state of the projectile. The target recoil takes up the excess momentum. At medium and high collision energies ($\eta \geqslant 1$), only the most strongly bound target electrons determine the total NRC cross-section. In general, a precise theoretical description is difficult, as the Coulomb field of the projectile leads to distortions of the atomic wave functions in the target even at infinite distances. However, already the simple first order OBK approximation gives the non-relativistic cross-section scaling dependence:

$$\sigma_{\text{NRC}} \sim \frac{Z_P^5 Z_T^5}{E_{\text{kin}}^5}. \tag{7}$$

In the relativistic regime, the energy dependence approaches asymptotically a $1/E_{\text{kin}}$-dependence [32].

The strong dependence of the NRC cross-section on the nuclear charges of the projectile and the target implies that at not too high energies this is by far the dominant capture process in collisions of high-Z projectiles with medium or high-Z target atoms. As discussed in detail by Eichler and Meyerhof [32], a reliable cross-section prediction from non-relativistic to relativistic energies can be obtained on the basis of the relativistic eikonal approximation.

Eichler [36] has derived an approximate analytical equation which allows the calculation of NRC cross-sections averaged over the subshells of arbitrary initial and final principal states $n(P)$. In particular, for low-Z targets, these predictions are well confirmed by experiments and one can estimate that this theory provides reliable predictions within a factor of two. In Fig. 5, the total cross-sections for electron pick-up from a N_2 gasjet target into bare uranium ions, measured at the ESR storage ring, are displayed. The data cover the projectile energy range from 50 to 360 MeV/u [25]. The

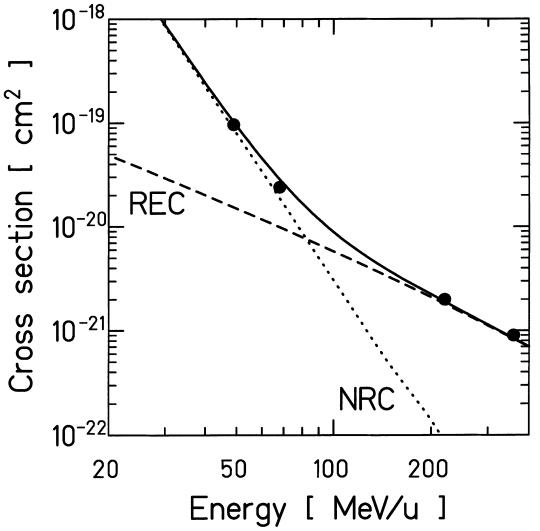

Fig. 5. Total one-electron-capture cross section of bare uranium ions in collision with N_2 molecules. The solid curve is the sum of the radiative (dashed curve) and non-radiative (dotted curve) electron-capture cross sections, which have been calculated using the dipole and eikonal approximations, respectively. The experimental data were measured at the ESR gas target [25].

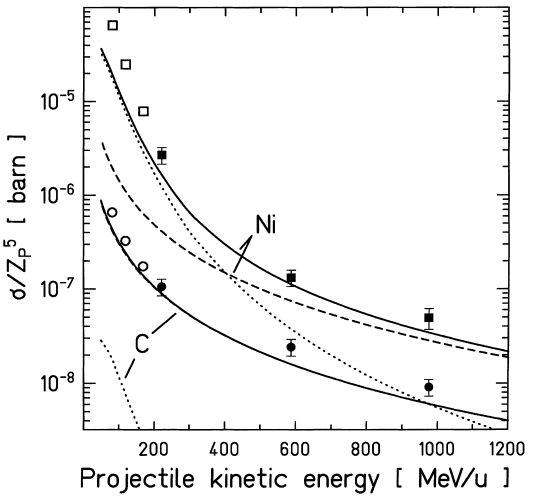

Fig. 6. Measured total electron capture cross sections for H-like Au (solid symbols) and Bi projectiles (open symbols) in C (circles) and Ni (squares) targets compared with theoretical predictions [12,22]. REC has been calculated in the dipole approximation (dashed curves), NRC has been calculated in the eikonal approximation (dotted curves). The total cross section (solid curves) is the sum of REC and NRC, and for C targets the solid line almost coincides with the dashed line. The calculations are shown only for Bi.

solid curve is the sum of cross-section calculations for REC (dipole-approximation) and the eikonal approach for NRC. The calculation takes into account the capture of the nitrogen K-shell electrons into projectile states up to $n(P) = 20$. Good agreement between experiment and theory is obtained, illustrating the different energy dependencies of NRC and REC.

Depending on the projectile nuclear charge, in narrow energy regions resonant transfer and excitation processes may become additional important electron capture mechanisms [37]. As an example, for resonant K-electron excitation of Xe, Au, and U, the main resonances lie in the energy range 30–40, 80–100, and 110–150 MeV/u. However, this resonant capture process will not be considered in this paper.

In Fig. 6, the comparison between experiment and theory is extended to capture cross-sections for Au^{78+} and Bi^{82+} ions colliding with C-targets and Ni-targets [12,22]. Here, both, the predicted scaling of the total capture cross-section with the nuclear charge of the targets and with the beam energy is confirmed by the experiments.

3. Models

In this section, models are described, which are useful for charge-state preparations and predictions for relativistic heavy ions [32].

Although it is common to label ionic ground states by their charge q, for the present purpose it is more convenient to label them by the number of electrons $n = Z_P - q$ on the ion, where Z_P is the projectile atomic number.

Many problems related to the statistics of the transport of an ion beam penetrating through layers of matter can be described analytically and efficiently with the Bothe–Landau scheme [38]. General expressions for energy-loss distributions, Coulomb-scattering distributions, and the charge-state spectrum of charged-particle beams as a function of target thickness have been given

by Sigmund [39]. Contributions from the collision and from deexcitation are treated within the framework of a matrix formalism which is outlined in Ref. [6].

Basic assumptions for the applicability of the transport equations to the specific case of charge-state distributions are (i) that the cross-sections leading to transitions between projectile states do not depend on the penetration depth, i.e., the slowing down of projectiles is neglected, and (ii) that the transition probabilities obey Poisson statistics. From Sigmund's treatment, the usual rate equations for the yield $Y_n(x)$ of projectile ions in state n can be retrieved:

$$\frac{\mathrm{d}Y_n(x)}{\mathrm{d}x} = \sum_{n' \neq n} \sigma(n', n) Y_{n'}(x) - \sigma_{\mathrm{tot}}(n) Y_n(x). \tag{8}$$

Here, x is the penetration depth (expressed in atoms/cm^2) in the target, $\sigma(n, n')$ is the cross-section (in cm^2) for a transition from projectile state n to state n', and

$$\sigma_{\mathrm{tot}}(n) = \sum_{n' \neq n} \sigma(n, n') \tag{9}$$

is the total charge-changing cross-section for an ion with n initially attached electrons. The sum $\sum_n Y_n(x)$ is normalized to unity.

Once the cross-sections $\sigma(n, n')$ are known, the charge-state fractions $Y_n(x)$ of ions with n electrons at a distance x in the target medium can be evaluated from the set of Eqs. (8). In practice, to solve Eq. (8), one has to limit the number of excited states. A typical calculation is that of Betz and Höppler [40]. Their model includes ions with up to seven electrons, distributed over 20 states among which 157 different transitions can occur.

Rozet [41] has developed a computer program based on an independent-electron model with up to 28 electrons on the ion, which can be distributed over the 1s, 2s, 2p, 3s, 3p, and 3d subshells. The model takes into account electron loss, capture, and excitation from and to all the subshells. It uses non-relativistic cross-sections adjusted to the energy of the ion at the location in the target where the particular collision occurs. For non-relativistic collisions, we have found the program ETACHA developed by Rozet [41] to be very accurate up to energies of 30 MeV/u. Unfortunately, in the energy range between ~30 and 100 MeV/u, at present no program provides reliable predictions.

In many cases of relativistic collisions it is not necessary to use such refined models. Especially in heavy projectiles, the relevant electronic transitions typically are so fast that the contributing (inner) electrons are in their ground state by the time the next collision occurs. If this is not the case, it is possible to take into account the most important excited-state effects through the use of effective ground-state cross-sections. Such a model is described in Ref. [18] and is discussed in Section 3.4.

Furthermore, spontaneous processes such as Auger decay of multiply excited ions upon leaving a solid [42] appear to be very small and can thus safely be neglected in the present context.

3.1. Ground-state model

The most important cross-sections are those for one-electron loss and capture, respectively given by

$$\sigma(n, n-1) = n_{\mathrm{K}} \sigma^{\mathrm{l}}_{\mathrm{K}} + n_{\mathrm{L}} \sigma^{\mathrm{l}}_{\mathrm{L}} + n_{\mathrm{M}} \sigma^{\mathrm{l}}_{\mathrm{M}}, \tag{10}$$

and

$$\sigma(n, n+1) = \frac{2 - n_{\mathrm{K}}}{2} \sigma^{\mathrm{c}}_{\mathrm{K}} + \frac{8 - n_{\mathrm{L}}}{8} \sigma^{\mathrm{c}}_{\mathrm{L}} + \frac{18 - n_{\mathrm{M}}}{18} \sigma^{\mathrm{c}}_{\mathrm{M}} + \sigma^{\mathrm{c}}_{\mathrm{H}}. \tag{11}$$

These relations assume that the ion carries at most 28 electrons which fill the shells in succession up to the M-shell, with n_{X} electrons in shell X, so that $n = n_{\mathrm{K}} + n_{\mathrm{L}} + n_{\mathrm{M}}$. In principle, each n_{X} can take values from zero up to the maximum number of electrons in the shell. The cross-section $\sigma^{\mathrm{l}}_{\mathrm{X}}$ is the loss cross-section for a single electron in shell X; for simplicity, Eq. (10) assumes that this cross-section does not vary with n, although such effects can be taken into account (see Section 3.4). The cross-section $\sigma^{\mathrm{c}}_{\mathrm{X}}$ is the non-radiative plus radiative capture cross-section from all filled target states into a completely vacant projectile shell X, again assumed to be independent of n, and $\sigma^{\mathrm{c}}_{\mathrm{H}}$ is the capture cross-section into all shells higher than M.

Similar to Eqs. (10) and (11), one can write expressions for $\sigma(n, n \pm m)$ in terms of the m-fold multiple-attachment and stripping cross-section,

respectively. Unless simplifying assumptions are made, these expressions are quite complicated because multiple processes in a single collision can involve more than one shell [18]. Fortunately, cross-sections decrease rapidly with increasing multiplicity, typically by an order of magnitude for each unit increase in multiplicity, so that multiple processes can be neglected.

Even with these simplifying assumptions the set of Eqs. (8) is not easily solved in general, because for projectiles of atomic number Z_P it involves $(Z_P+2)(Z_P+1)$ cross-sections, assuming that the negative ion with (Z_P+1) electrons is stable. Therefore, it is appropriate to examine still more restricted model solutions.

3.2. Pure stripping model

For heavy projectiles of several hundred MeV/u energy and for light stripper foils, approximately up to $Z_T \leqslant 13$, capture is negligible compared to loss for the M-, L-, and possibly K-shells of the ions. If one also neglects multiple stripping compared to one-electron stripping, a simple statistical argument provides an analytical solution to Eq. (8). From this solution, the choice of stripper thickness for maximum yield of the desired charge state can be obtained, as well as the width of the charge state distribution [43]. If stripping takes place only within one shell (M, L, or K), the expressions are particularly simple. A small amount of capture does not affect the results significantly, except at thicknesses close to charge-state equilibrium, so that the results can be of practical value.

We start with a schematic one-shell model in which a n-electron ion has a one-electron stripping cross-section, given by Eq. (10),

$$\sigma(n, n-1) = n\sigma^{1}, \tag{12}$$

where σ^1 is the average loss cross-section per electron. On traversing a thickness x in the target medium, an electron has the probability

$$\tau = \mathrm{e}^{-\sigma^{1}x} \tag{13}$$

of surviving on the ion and $(1-\tau)$ to be stripped. Hence, if the ion enters with N electrons, the probability that just n electrons survive on the ion at x is given by the binomial expression

$$Y_n(x) = \frac{N!}{n!(N-n)!}\tau^n\ (1-\tau)^{N-n}. \tag{14}$$

By substitution, one finds that Eq. (14) is a solution of Eq. (8) which satisfies $\sum_{n=0}^{N} Y_n(x) = 1$.

From Eq. (14), one concludes that the mean number of electrons $\overline{n}$ on the ion is

$$\overline{n} = N\tau. \tag{15}$$

Also, one can show that at $\tau = \overline{n}/N$, $Y_n[x(\tau)]$ has a maximum at $n = \overline{n}$ given by

$$Y_{\overline{n}} \simeq \left[\frac{N}{2\pi\overline{n}(N-\overline{n})}\right]^{1/2}, \tag{16}$$

where Stirling's approximation has been used for each factorial in Eq. (14).

For the more realistic case of an ion with electrons in several shells X, it is convenient to write the cross-section for one-electron stripping, Eq. (10), in the form

$$\sigma(n, n-1) = (n_X + g_X)\sigma^{1}_{X}, \tag{17}$$

where, for the M-shell,

$$g_M = (8\sigma^{1}_{L} + 2\sigma^{1}_{K})/\sigma^{1}_{M}, \tag{18}$$

for the L-shell,

$$g_L = 2\sigma^{1}_{K}/\sigma^{1}_{L}, \tag{19}$$

and

$$g_K = 0. \tag{20}$$

Eq. (14) still gives the correct result for stripping within one shell, if one substitutes

$$N \to N_X + g_X \quad \text{and} \quad n \to n_X + g_X, \tag{21}$$

where N_X is the initial number of electrons in shell X. For typical relativistic ions, one finds $g_M \simeq 2$–3 and $g_L \simeq 0.2$–0.3. Substitution into Eq. (16) then gives peak values $Y_{\overline{n}} \simeq 0.2$ or 0.3 for stripping to the middle of the M- or L-shells, respectively. For stripping to $\overline{n}_M = 0$ or $\overline{n}_L = 0$, Eq. (14) shows that peak values $Y_{\overline{n}} \simeq 0.6$ can be obtained. These maximum yields are independent of Z_T ($\leqslant 13$), Z_P, or ion velocity v, except through a slight Z_P and v dependence of g_X. Of course, to obtain a peak yield at a desired value of $\overline{n}_X$, the stripper foil thickness must be chosen so that Eq. (15), with the substitutions (21), is fulfilled. For this purpose, the stripping cross-sections must be known.

3.3. Equilibrium ground-state model

Before discussing general non-equilibrium solutions of Eq. (8), we turn to the equilibrium solutions, obtained by setting $dY_n(x)/dx = 0$. These solutions are treated in detail by Betz [4]. We restrict the discussion to relativistic collisions where for the present purpose one can neglect multiple processes. Then, one finds that the equilibrium fractions F_n of Eq. (8) obey the iterative relation

$$F_{n+1}\sigma(n+1,n) = F_n\sigma(n,n+1), \tag{22}$$

where the definitions of Eqs. (10) and (11) for the one-electron stripping and attachment cross-sections are used. The relation (22) is most easily derived by starting with $n = 0$ or $n = Z_P$ and iterating Eq. (8) step by step, with the condition $dY_n(x)/dx = 0$.

To solve Eq. (22), it is convenient to write it in the form

$$F_n = r_n F_{n+1}, \tag{23}$$

where

$$r_n = \sigma(n+1,n)/\sigma(n,n+1). \tag{24}$$

Iterating Eq. (23) from F_n to F_{Z_P} (which represents the – minute – equilibrium fraction of neutral projectile atoms), one finds

$$F_n = r_n r_{n+1} \ldots r_{Z_P-1} F_{Z_P}, \tag{25}$$

where

$$F_{Z_P} = \left(1 + \sum_{n'=0}^{Z_P-1} r_{n'} r_{n'+1} \ldots r_{Z_P-1}\right)^{-1}. \tag{26}$$

Since (i) $F_{Z_P} \ll 1$, so that unity can be neglected with respect to the sum in Eq. (26), and (ii) $r_n \gg 1$ until $n = 2$ is reached, one finds that

$$(F_{Z_P})^{-1} \simeq r_{Z_P-1} r_{Z_P-2} r_{Z_P-3} \ldots r_2[1 + r_1(1 + r_0)]. \tag{27}$$

Using Eq. (25), one can now compute any F_n, in particular the two-electron, one-electron, and bare-ion yields

$$F_2 = 1/D, \qquad F_1 = r_1/D, \qquad F_0 = r_1 r_0/D, \tag{28}$$

where

$$D = 1 + r_1 + r_1 r_0. \tag{29}$$

From Eq. (24) one obtains

$$r_1 = \frac{2\sigma_K^l}{\sigma(0,1) - \sigma_K^c/2}, \tag{30}$$

$$r_0 = \frac{\sigma_K^l}{\sigma(0,1)}. \tag{31}$$

Here, σ_K^l is the loss cross-section for a single electron in the projectile K-shell, $\sigma(0,1)$ is the one-electron attachment cross-section into the bare projectile from all filled target shells, and σ_K^c is the capture cross-section into the empty K-shell.

The minimum foil thickness necessary to produce charge-state equilibrium, to a good approximation is given by the expression [44]

$$x_{eq} \simeq \frac{4.6}{\sigma_K^l + \sigma(0,1)/2}, \tag{32}$$

although the relation $x_{eq} \simeq 1/\sigma_K^l$ has also been proposed [45]. In numerical calculations the equilibrium thickness can be determined by requiring that the relative variation of the charge-state fractions with penetrated thickness approaches zero.

3.4. Quasiground-state model

As noted above, in a solid, excited-state effects can occur which are not always negligible. This has two consequences. (i) Capture to excited states will be reduced if these states are still occupied when the next collision occurs. Hence, the effective attachment cross-section to higher states is reduced. (ii) There can be electron loss from occupied excited states. Then, the effective ground-state stripping cross-section is increased, since the loss cross-section from an excited state is larger than that from the ground state.

These qualitative statements have been quantified in calculations by Anholt, first, assuming an ion in which one electron can occupy the 1s, 2s, or 2p states, or be absent [15], and, second, allowing two electrons to occupy these states [18]. Since the former case is more transparent than the latter, we restrict the discussion to it.

From Eq. (6) of Ref. [15], one can show that the equilibrium ratio F_1/F_0 of one-electron to bare ions can be written in the form

$$F_1/F_0 = \sigma^c(\text{eff})/\sigma^s(\text{eff}), \quad (33)$$

where the effective attachment cross-section is

$$\sigma^c(\text{eff}) = \sigma(0,1) - f\sigma(1,2) \quad (34)$$

and the effective stripping cross-section is

$$\sigma^l(\text{eff}) = \sigma^l_K + f\sigma^{tot}_{ex}. \quad (35)$$

Here, the same notation is used as in Eq. (31), $\sigma(1,2)$ is the one-electron attachment cross-section for the one-electron ion, and σ^{tot}_{ex} is the total (to a good approximation, 1s→2s plus 1s → 2p) excitation cross-section from the one-electron ground state. The factor f is less than unity and is given by

$$f = (\sigma^l_L - \sigma^l_K)/(\sigma^l_L + \sigma_{de} + \sigma^{tot}_{ex}), \quad (36)$$

where the cross-section σ_{de} represents a radiative and collisional deexcitation cross-section given by

$$\sigma_{de} = \frac{3}{4}\frac{\lambda(2p \to 1s)}{n_T \gamma v} + \frac{1}{4}\sigma_{ex}(1s \to 2p). \quad (37)$$

Here, $\lambda(2p \to 1s)$ is the 2p→1s radiative decay constant, n_T is the number of target atoms per unit volume, v is the projectile velocity ($\simeq c$), and γ is the projectile Lorentz factor.

If the deexcitation process dominates, $f \to 0$ and the ratio (33) reduces to the ground-state model value obtained from Eq. (28)

$$(F_1/F_0)_{gs} = \sigma(0,1)/\sigma^l_K. \quad (38)$$

On the other hand, if deexcitation is small, as might be the case if metastable states are formed, there can be noticeable excited-state effects.

3.5. Three charge-state model

The three charge-state model of Allison [5] is very useful in cases where either the heavy-ion velocity and charge state is high enough that only three charge states occur or if soon upon entering the target medium, the projectile is stripped down to the K-shell. In practice, it is usually applicable if the Bohr criterion (Section 1) is fulfilled for K-shell electrons. As shown by Allison [5], for three charge states the rate Eqs. (8) can be easily solved analytically. Applied to electrons in the K-shell, this model includes the multiple cross-sections $\sigma(2,0)$ and $\sigma(0,2)$ and provides the complete solutions of Eq. (8) for a maximum number of two electrons on the projectile. Using the present notation, the solutions are of the form

$$Y_n(x) = F_n + [A(N,n)e^{\zeta x} + B(N,n)e^{-\zeta x}]e^{\sigma_{TOT}x/2}. \quad (39)$$

Here, F_n is the equilibrium charge-state fraction, which is obtained in the limit $x \to \infty$, i.e., by neglect of energy loss of the projectile. The quantities A and B depend on the initial electron number N $(= 0, 1, 2)$ on the ion, as well as on n. The quantity ζ is a function of the cross-sections; it, as well as A and B, is listed in Ref. [5] (care must be taken to change from the charge-state to the electron-number notation). The cross-section $\sigma_{TOT} = \sum_n \sigma_{tot}(n)$, where $\sigma_{tot}(n)$ is defined in Eq. (9).

The F_n's can be obtained directly from the cross-sections. If multiple processes can be neglected, the expressions for the F_n's are identical to Eq. (28) [assuming $\sigma(2,1) = 2\sigma^l_K$, $\sigma(1,0) = \sigma^l_K$]. For the case of pure stripping, the solutions (39) reduce to Eq. (14) ($N \leqslant 2$). This model reduces to a two charge-state model if cross-sections involving the third charge state vanish.

4. The codes CHARGE and GLOBAL

Over the last decade, we have developed two different computer codes which provide solutions of Eq. (8) for relativistic collisions ($E/A \geqslant 100$ MeV/u) of heavy projectiles ($Z_P \geqslant 30$). In this section, we outline their features and the used approximations.

The code CHARGE [46] uses the analytical solutions of Allison's [5] three-state model and is thus restricted to describe the charge-state evolution in the high-energy domain where only bare, H-, and He-like ions occur. The cross-sections for projectile ionization are calculated according to Eq. (4) and screening is taken into account by means of the Slater screening constants [47]. Electron capture cross-sections are calculated according to Section 2.2. The NRC cross-section is obtained by summing up over all projectile principal quantum numbers up to 10 and over all target principal quantum numbers up to 3, the REC cross-section is calculated using the Stobbe formula [33]. Rough estimates for double processes are

made by assuming the double capture cross-section to be one tenth of the NRC cross-section into the bare projectile and by assuming the double ionization cross-section to be one tenth of the single-ionization of the H-like projectile.

The code GLOBAL [48] takes into account up to 28 charge states. As noted by Betz [4], the most useful numerical method for solving Eq. (8) is the Runge–Kutta method [49]. The main task is to parameterize the cross-sections $\sigma(n, n')$ in such a way that they are useful over the widest range of applicability.

Eq. (10) is used for the stripping cross-section. To obtain the cross-section for the different shells and subshells, the K-shell binding energy E_K in Eq. (10) is replaced by the ionic binding energy E_X of shell or subshell X taken from Ref. [50]. In the program, screening effects are taken into account by interpolating each σ_X^l linearly between its "unscreened" value (corresponding to the $1s^2$ 2s or $1s^2$ $2s^2$ $2p^6$ 3s electron configurations for the L- or M-shells, respectively) and its "screened" value (corresponding to the $1s^2$ $2s^2$ $2p^6$ or $1s^2$ $2s^2$ $2p^6$ $3s^2$ $3d^6$ $3d^{10}$ configurations), as each shell is filled. Double K- and L-shell loss are taken into account schematically, using the work of Ref. [27].

Eq. (11) is used for the attachment cross-sections. Each non-radiative capture cross-section σ_X^c is computed with the eikonal approximation, using the analytical K-shell formula derived by Eichler [37] and adapted to other shells in Ref. [16]. Screening effects are taken into account in a manner similar as for σ_X^l. The radiative electron capture cross-section is taken as a mean between the Sauter and Bethe-Salpeter cross-sections [23]. Double and triple capture are considered schematically, using the work of Ref. [27].

Excited-state effects are treated in an approximate manner by modifying the stripping and attachment cross-sections consistent with Eqs. (35) and (34), respectively. In principle, these modification are appropriate only for the equilibrium situation. But, the work of Ref. [18] suggests that excited-state effects are not important at small target thicknesses. A further compromise is made by modifying only the K- and L-shell cross-sections for excited-state effects, since these cross-sections play a more important role at larger target thicknesses. On the other hand, at small target thicknesses, the M-shell stripping is not well represented by the model (see Section 5.1).

Using fitted range-energy relations, the program GLOBAL is able to determine the projectile energy at a certain penetration depth in the target. This allows the ionization and capture cross-sections to be adjusted to the projectile energy at the point of collision. The adjustment is specially important for thick targets, where the continuous change of projectile energy can prevent the attainment of a charge-state-equilibrium situation (see Fig. 11).

5. Comparison with experiment

In the following sections we compare the predictions of CHARGE and GLOBAL with experimental data measured at GSI (Darmstadt) and at LBL (Berkeley). By applying the program to over one hundred collision systems with $54 \leqslant Z_P \leqslant 92$ and $4 \leqslant Z_T \leqslant 92$ for which experimental data are available from LBL and GSI, we have found that at collision energies in excess of ~100 MeV/u the charge state yields generally are predicted to better than a factor of two. The exceptions are mostly in the electron number range in which stripping in the M shell takes place (see below). For small charge-state yields of the order of one percent or less, the predictions can deviate more from experiment. Few experimental data are available for lighter projectiles at relativistic energies because there the projectiles are nearly completely stripped [15].

The following examples have been selected to give representative results for light, medium heavy, and very heavy targets and medium and very heavy projectiles with kinetic energies from about 80 to 1000 MeV/u.

5.1. Non-equilibrium distributions

In Figs. 7–11 the calculated evolution of various charge-state distributions with target thickness is presented and compared with experimental data. Figs. 7 and 8 depict the charge-state evolutions for the ions Au and U at about 1 GeV/u in three

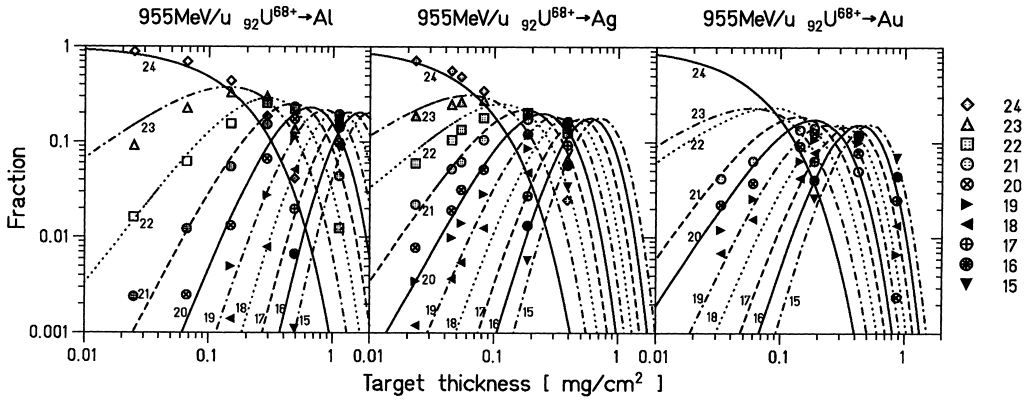

Fig. 7. Charge-state evolution as a function of target thickness for 955-MeV/u U^{68+} ions in thin Al, Ag, and Au targets impinging with 24 electrons. The lines represent the predictions of GLOBAL. The numbers written next to the lines denote the electron number n on the projectile. If not explicitly defined otherwise, throughout this paper solid lines are used for $n = 0, 4, 8, \ldots$, dashed lines for $n = 1, 5, 9, \ldots$, dotted lines for $n = 2, 6, 10, \ldots$, and dash-dotted lines for $n = 3, 7, 11, \ldots$, respectively.

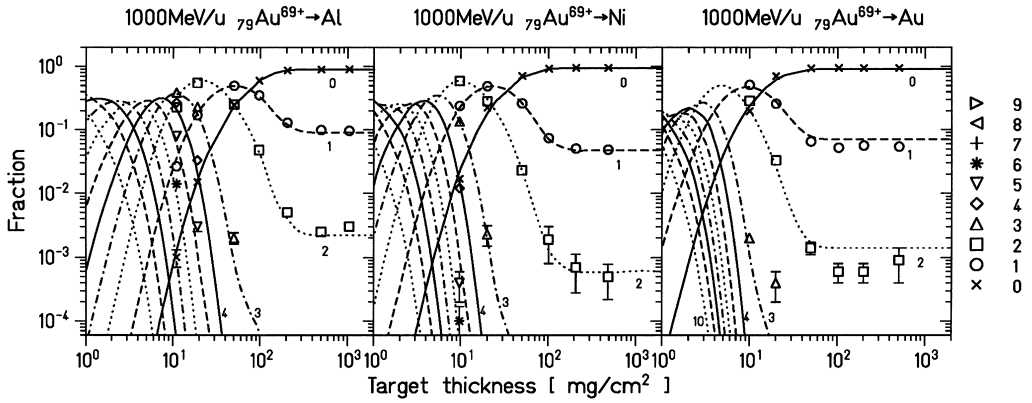

Fig. 8. Charge-state evolution of 1000-MeV/u Ne-like Au ions impinging on Al, Ni, and Au targets. Due to the much larger cross sections in high-Z materials, charge-state equilibrium in Au targets is reached much earlier than in Al and Ni [22]. The curves are the results of GLOBAL. The symbols used for the experimental data denote the electron number n attached to the projectile and are used from now on throughout the paper with the same meaning.

different target materials. For comparison, Fig. 9 shows examples for Xe projectiles at lower energies.

The dependence of the charge-state distributions on the electron number turns out to be the most sensitive test of the predictive power of model calculations. In Fig. 10 we present two measured thin-target charge-state distributions which are typical of stripping in the M and L-shells, respectively. As mentioned previously, the predicted M-shell distribution is only in qualitative agreement with experiment, whereas the predicted L-shell distribution is quite accurate.

Fig. 11 is an example for the charge-state evolution of bare projectiles (U) impinging on thick targets (Ti). The displayed theoretical curves are calculated with CHARGE and are almost identical with the predictions of GLOBAL. As can be seen from the figure, in very thick targets the energy loss is considerable, thus affecting

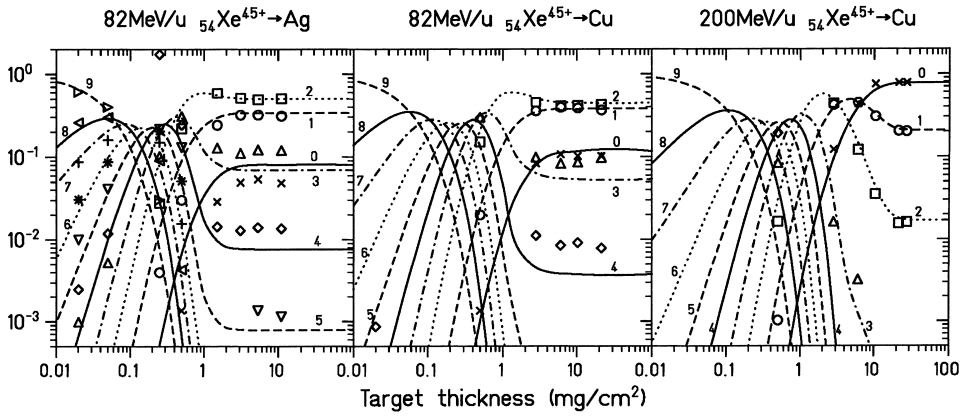

Fig. 9. Charge-state evolution of 82-MeV/u F-like Xe ions in Ag and in Cu, respectively, and of 200-MeV/u F-like Xe ions in Cu. Here, the energy loss of the projectiles in the target was not taken into account in the calculations using the program GLOBAL. The symbols have the same meaning as in Fig. 8.

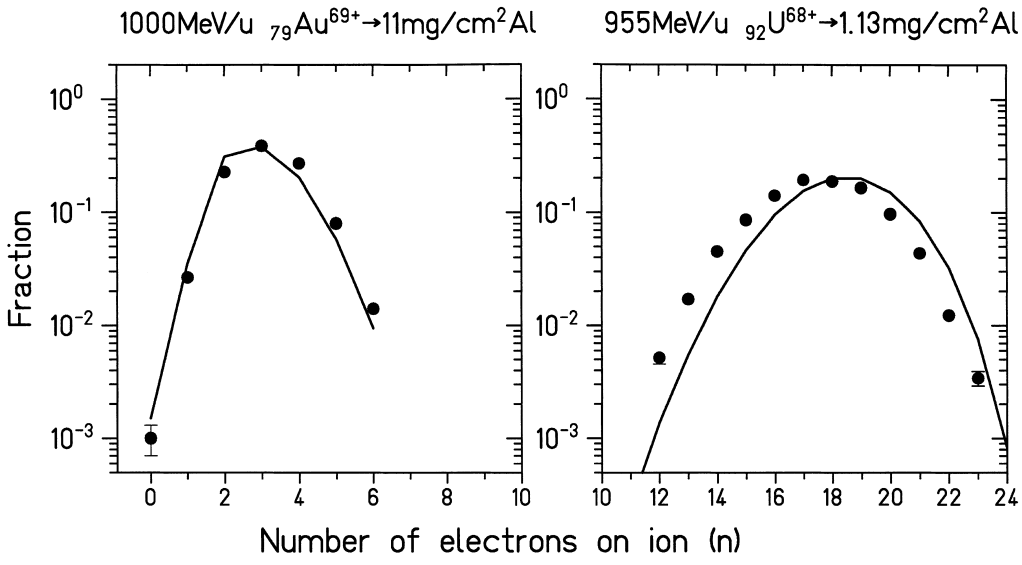

Fig. 10. Calculated (solid line) and measured (full circles) charge-state distribution for stripping as a function of the number of electrons on the emerging projectile. Left: 1000-MeV/u Au^{69+} impinging on 11-mg/cm^2 Al. Right: 955-MeV/u U^{68+} ions behind 1.13-mg/cm^2 Al.

charge-changing cross-sections and charge-state distributions. While GLOBAL takes into account the slowing-down automatically, CHARGE calculations require the corresponding energy as user input.

On the whole, the predictions of GLOBAL and CHARGE agree with experiment to better than a factor of two. Therefore, these programs are quite well suited for stripper design and for other applications.

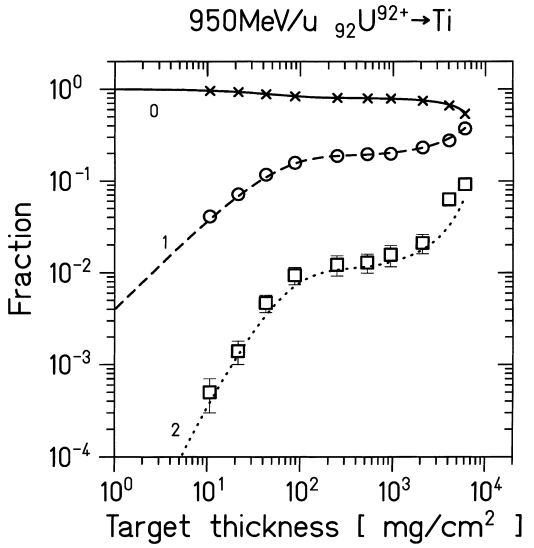

Fig. 11. Charge-state evolution of 950-MeV/u bare U ions impinging on Ti targets. Here, the three-state program CHARGE is sufficient to describe the measured data, and gives essentially the same results as the program GLOBAL. For very large target thicknesses, the slowing down of the projectile must be taken into account.

5.2. Equilibrium distributions and equilibrium thicknesses

Figs. 12 and 13 give predictions of GLOBAL for equilibrium charge-state distributions, as a function of target atomic number and projectile energy, respectively. In general, the predictions are very satisfactory. The results of CHARGE coincide almost with those of GLOBAL as long as as only bare, H-, and He-like ions are observed. From experience, we can conclude that CHARGE gives reliable predictions as long as the He-like fraction is approximately equal to or smaller than the bare-ion fraction.

The equilibrium charge-state distributions for the collision systems shown in Fig. 10 (Au and U in Al) are displayed as a function of electron number in Fig. 14. Here, the model calculations represent the data very well, even at low energies where many charge-states contribute to the equilibrium distribution.

We complete this survey with a prediction of the target thicknesses required to achieve charge-state equilibrium for heavy projectiles. Fig. 15 shows calculated equilibrium thicknesses of C, Cu, and Au targets. Finally, we present calculated equilibrium charge-state distributions for Xe, Dy, Au, U ions in various target materials in Table 1.

6. Limitations of the models

Despite the good overall agreement between experimental data and the predictions obtained from CHARGE and GLOBAL, certain limitations of the applied charge-state models must be stressed. Electron-correlation processes such as resonant transfer and excitation (RTE), i. e., the time-reversed Auger effect, are not considered. RTE takes place when the adiabaticity parameter η is smaller than unity, and may enhance considerably the electron capture cross-sections in low-Z targets. Consequently, for stripper targets such as Be or C, this may have large impact on the charge state distribution.

In general, in the computer codes only approximations are used which were derived from first order perturbation theories (see Section 2). This implies, that in particular for symmetric collision systems, where high-Z targets and high-Z projectiles are involved, the calculated charge-exchange cross-sections are questionable. Moreover, since we are essentially dealing with relativistic collisions of high-Z projectiles in the β regime between 0.4 and 0.9, relativistic effects start to play an important role. However, most of the charge-exchange cross-sections are calculated by using non-relativistic theories and relativistic effects are added in an approximate way. In some particular cases, e.g., K-shell excitation to p-levels, this may lead to deviations from more appropriate theories by a factor of two [24].

Summarizing the various limitations of the applied models, we emphasize that the aim of the developed computer codes is to provide a reasonable basis for the prediction of charge-state evolutions and distributions in matter. The cross-sections calculated by CHARGE and GLOBAL should be interpreted as effective cross-sections for high-Z ions interacting with solid matter rather than precise

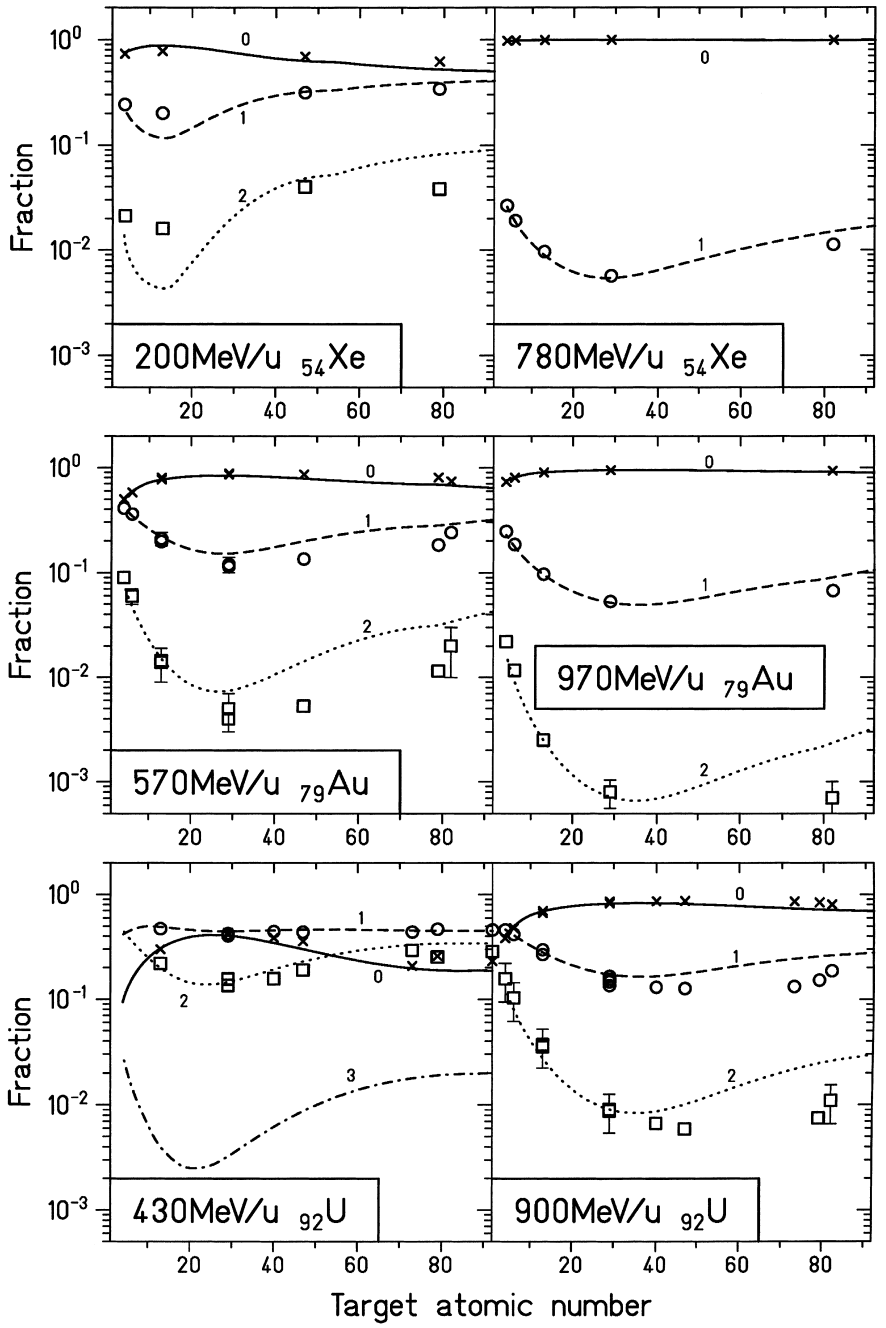

Fig. 12. Calculated and measured equilibrium charge-state distributions of Xe, Au, and U projectiles at different energies in various target materials. The curves are predictions of GLOBAL, which almost coincide with the predictions of CHARGE.

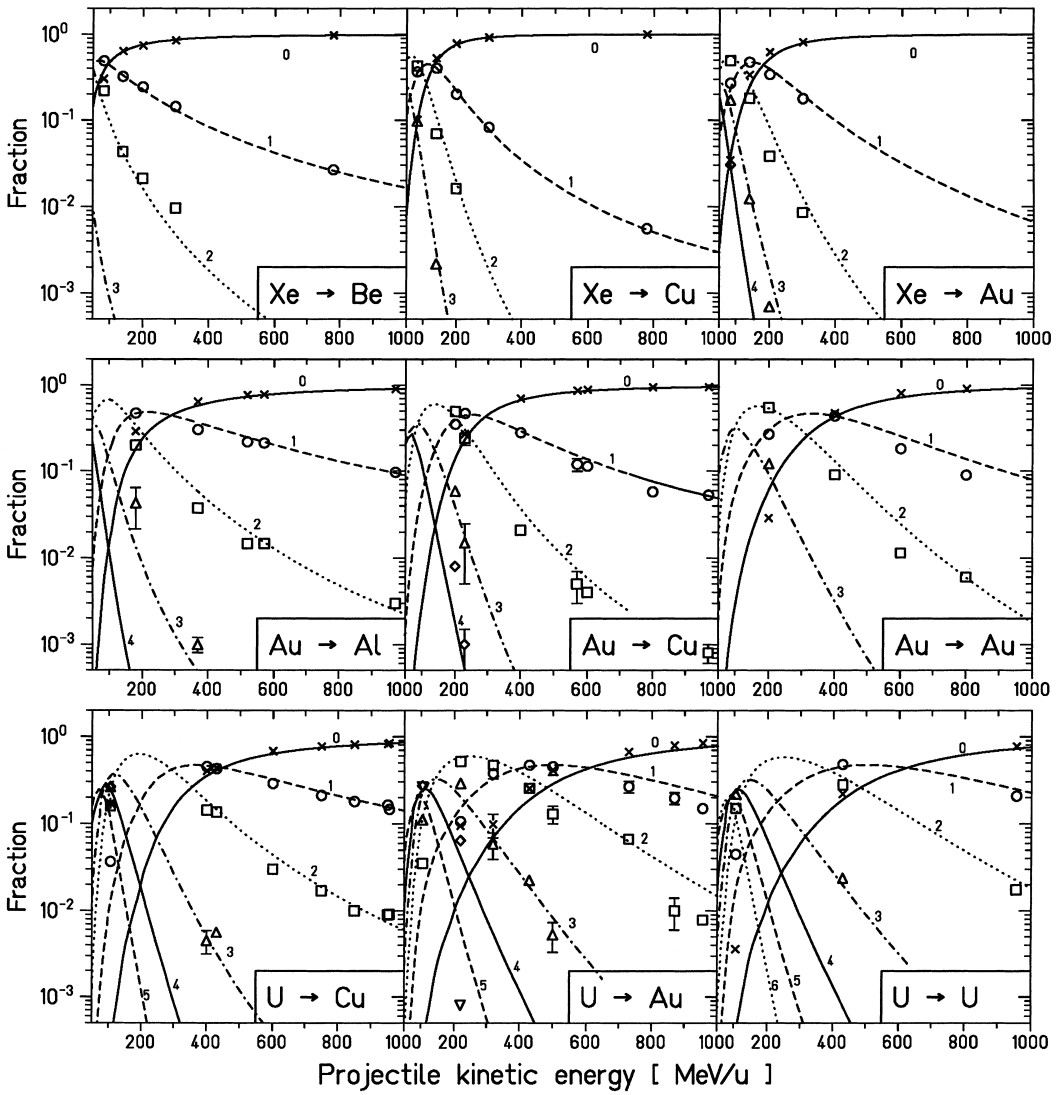

Fig. 13. Calculated and measured equilibrium charge-state distributions of Xe, Au, and U projectiles in various target materials displayed as a function of the projectile energy. The curves are predicted by GLOBAL.

predictions of cross-sections for all atomic collision processes under single-collision conditions.

7. Applications

We illustrate a typical application by discussing the design of a stripper used at the CERN Pb-beam project [51]. The problem is to chose the best material and the optimum thickness for a stripper placed between PS and SPS accelerators at CERN. The incident beam (extracted from the PS) is 4.25 GeV/u Pb^{53+}. Behind the stripper, the ions should be fully stripped in order to reach the highest possible energy in the subsequent accelerator SPS. In addition, transverse and longitudinal

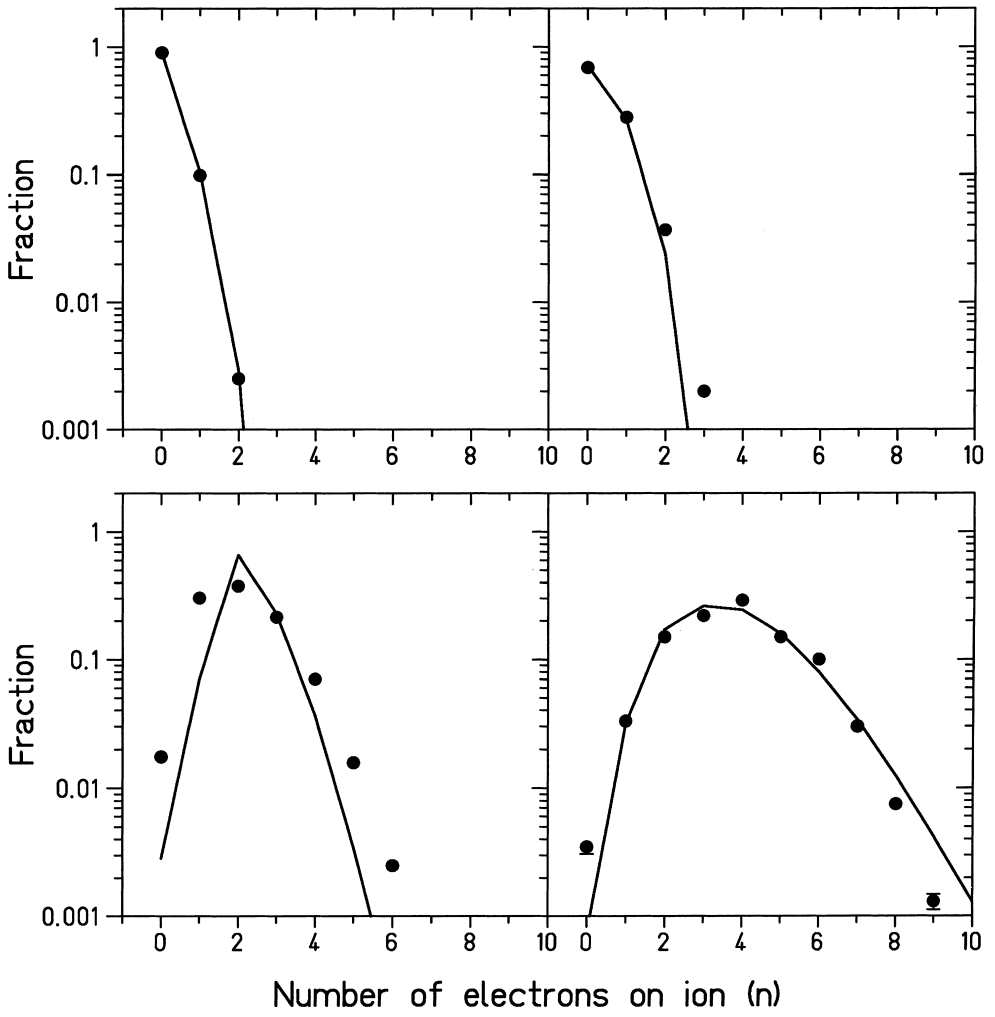

Fig. 14. Calculated (solid lines) and measured (full circles) charge-state distributions for stripping as a function of the number of electrons on the emerging projectile: Upper left: 1000-MeV/u Au ions → 501-mg/cm^2 Al; upper right: 950-MeV/u U ions → 377-mg/cm^2 Al; lower left: 120-MeV/u Bi → 228 mg/cm^2 Al; lower right: 105-MeV/u U ions → 43-mg/cm^2 U.

emittance blow-up, i.e., angular and energy-loss straggling, respectively, should be small because of the restricted phase-space acceptance of the SPS.

The performance of several stripper materials ranging from Be to Au was investigated. Fig. 16 shows the calculated equilibrium thicknesses which are required to achieve the highest yield of bare ions. Except for Be and C, in all materials more than 99% of the ions become fully stripped. Since capture and ionization cross-sections scale with high powers of Z_T, in high-Z target materials the cross-sections are much larger than in low-Z materials. Therefore, in these materials, equilibrium conditions are reached at smaller target thicknesses and thinner strippers can be used.

The longitudinal emittance blow-up is governed by the energy-loss straggling. Although from this point of view a high-Z material would be advantageous (see lower part of Fig. 16), the energy-loss straggling [52] is negligible as compared to the

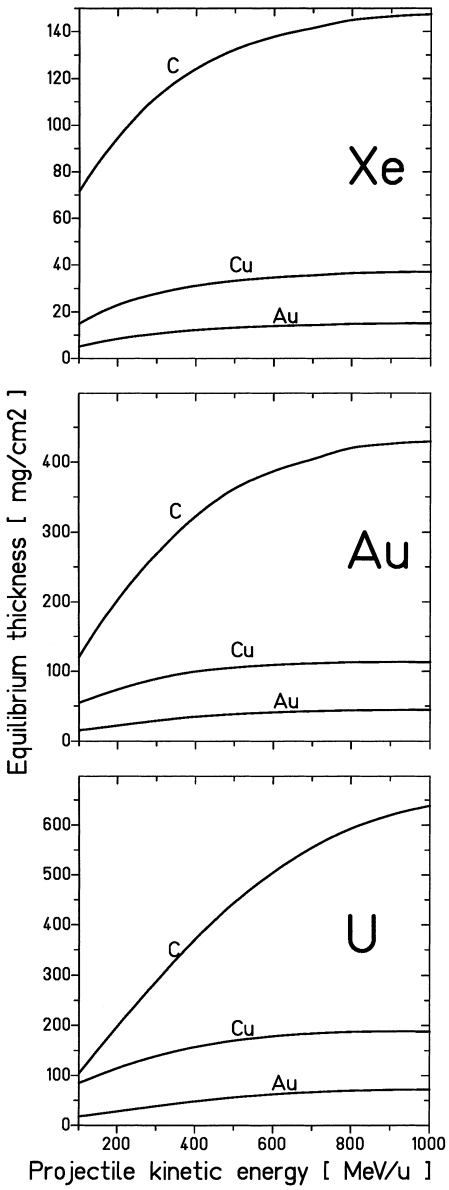

Fig. 15. Equilibrium thicknesses calculated according to Eq. (32) for Xe (upper part), Au (middle), and U (lower part) impinging on targets made of C, Cu, and Au, respectively, in the energy range (100 . . . 1000) MeV/u.

relative momentum spread of the beam (which is of the order of a few times 10^{-4} for the Pb beam extracted from the PS).

Multiple scattering, which determines the transverse emittance blow-up, increases with the atomic number of the penetrated material, but this increase is slightly overcompensated by the decreasing stripper thickness required for charge-state equilibrium. Therefore the transverse emittance growth depends only weakly on Z_T.

Finally, Al was chosen for the stripper because of practical considerations. Transmission measurements confirmed that a 1-mm-thick Al stripper has the best performance with respect to stripping efficiency and emittance blow-up [53].

8. Conclusions

From our measurements and the comparison with model predictions, we can conclude that in general charge-changing processes of highly-charged projectiles during their passage through matter are well understood to predict charge-state distributions in the energy range from 80 to 1000 MeV/u. A striking result is that even for the heaviest projectiles only few charge states occur at equilibrium conditions. In the modeling of charge-state evolutions, some simplifying assumptions can be made, such as the neglect of multiple processes and excited-state effects. This knowledge and experience has been implemented in the codes GLOBAL [48] and CHARGE [46], which are useful tools for charge-state predictions of relativistic heavy ions and for applications.

Acknowledgements

The authors thank B. Franzke who provided unpublished data, which are shown in Fig. 1. We would like to thank A. Heinz and A. Junghans who extensively tested the code GLOBAL and gave valuable comments on the practical use of the program. Special thanks are devoted to those who contributed to make the experiments a success: R. Anholt, F. Bosch, H. Irnich, C. Kozhuharov, A. Magel, R. Moshammer, F. Nickel, M. Pfützner, P. Rymuza, W. Schwab, Z. Stachura, J. Ullrich, B. Voss, and A. Warczak. The excellent support of the GSI target laboratory is gratefully acknowledged. We are indebted to G. Münzenberg for the good collaboration over many years.

Table 1
Calculated equilibrium thicknesses and charge-state distributions of Xe, Dy, Au, and U ions in Be, C, Al, Cu, Ag, and Au targets at various projectile kinetic energies E (in MeV/u)

	Projectiles in					
E	Be	C	Al	Cu	Ag	Au
Xenon projectiles						
	(90)	(64)	(35)	(10)	(5)	(3.3)
50	16:47:35:1:0	19:46:34:1:0	5:25:58:11:1	1:13:56:23:5	1:13:53:23:7	1:10:44:25:12
	(97)	(66)	(35)	(11)	(6)	(3.8)
65	28:50:22:0:0	34:47:18:0:0	18:41:38:3:0	4:25:56:12:2	3:23:57:14:2	2:19:55:17:5
	(105)	(71)	(38)	(13)	(7)	(4.6)
85	41:46:13:0:0	50:41:9:0:0	42:42:16:0:0	14:40:41:4:0	9:36:48:6:1	7:31:53:8:1
	(112)	(74)	(40)	(15)	(8)	(5.1)
100	49:42:9:0:0	58:36:6:0:0	55:36:8:0:0	24:45:29:2:0	16:43:37:3:0	12:39:44:4:1
	(130)	(86)	(45)	(20)	(11)	(6.9)
150	66:30:4:0:0	74:24:2:0:0	79:19:1:0:0	58:35:7:0:0	45:43:12:0:0	36:46:17:1:0
	(210)	(130)	(70)	(33)	(21)	(13.2)
500	93:7:0:0:0	94:6:0:0:0	97:3:0:0:0	98:2:0:0:0	96:4:0:0:0	94:6:0:0:0
Dysprosium projectiles						
	(115)	(93)	(67)	(24)	(8)	(6)
50	1:18:73:7:0	1:19:72:8:0	0:6:59:28:6	0:3:31:35:21	0:3:26:31:22	0:4:20:26:22
	(140)	(107)	(70)	(26)	(11)	(7)
75	6:35:56:3:0	8:39:51:2:0	5:26:59:9:1	1:12:56:24:6	1:11:53:26:8	1:12:47:26:10
	(165)	(120)	(76)	(30)	(13)	(8)
100	12:45:42:1:0	17:48:34:1:0	17:43:38:2:0	5:26:56:12:1	3:22:58:15:2	3:21:56:16:3
	(200)	(145)	(84)	(37)	(18)	(11)
150	26:50:23:1:0	35:48:17:0:0	46:42:12:0:0	25:45:28:2:0	15:42:40:3:0	12:39:44:4:0
	(270)	(180)	(100)	(47)	(27)	(16)
250	49:42:9:0:0	59:36:5:0:0	74:24:2:0:0	67:29:4:0:0	51:39:9:0:0	42:44:13:0:0
	(380)	(240)	(130)	(62)	(39)	(24)
600	83:16:1:0:0	87:13:0:0:0	93:7:0:0:0	95:5:0:0:0	93:6:0:0:0	89:10:0:0:0
Gold projectiles						
	(135)	(110)	(95)	(52)	(19)	(14)
70	0:8:75:15:1	0:10:75:13:1	0:5:61:27:5	0:2:26:35:23	0:2:22:31:24	0:4:20:28:23
	(170)	(140)	(110)	(57)	(23)	(15)
100	1:16:72:10:1	2:21:70:7:0	2:19:67:11:1	0:7:53:30:8	0:7:47:31:11	1:10:44:29:12
	(230)	(180)	(130)	(66)	(30)	(18)
150	4:31:60:5:0	7:37:53:3:0	12:42:43:2:0	5:27:57:10:1	3:22:59:14:2	3:22:57:15:3
	(290)	(225)	(150)	(75)	(38)	(22)
200	9:41:47:3:0	14:46:39:1:0	26:48:25:1	17:42:38:3:0	10:37:47:5:0	9:36:49:6:5
	(440)	(310)	(190)	(96)	(55)	(32)
350	27:50:22:1:0	36:48:16:0:0	56:38:6:0:0	61:33:6:0:0	48:41:11:0:0	39:45:16:0:0
	(620)	(410)	(225)	(111)	(70)	(43)
700	62:34:4:0:0	70:27:3:0:0	83:16:1:0:0	89:10:0:0:0	88:12:0:0:0	82:17:1:0:0
Uranium projectiles						
	(145)	(130)	(115)	(85)	(40)	(18)
100	0:4:62:28:5	0:5:69:22:3	0:5:62:27:5	0:1:26:36:24	0:2:21:32:25	0:2:17:27:25
	(210)	(180)	(155)	(100)	(50)	(23)
150	0:9:69:19:2	1:13:72:13:1	2:18:69:10:1	1:9:57:26:6	0:7:50:30:9	0:9:47:29:11
	(275)	(225)	(190)	(115)	(60)	(28)
200	1:16:69:13:1	2:23:66:8:0	5:33:57:4:0	3:22:61:12:1	2:18:60:17:2	2:17:59:18:3

Table 1 *(Continued)*

	Projectiles in					
E	Be	C	Al	Cu	Ag	Au
	(400)	(320)	(240)	(140)	(80)	(40)
300	4:30:59:6:0	7:37:52:4:0	16:47:35:1:0	19:44:35:2:0	12:39:44:4:0	8:35:51:6:0
	(640)	(470)	(310)	(170)	(100)	(56)
500	14:47:37:2:0	22:49:28:1:0	40:46:13:0:0	55:38:7:0:0	47:41:11:0:0	34:46:19:1:0
	(940)	(640)	(370)	(190)	(120)	(72)
1000	47:43:10:0:0	57:37:6:0:0	74:24:2:0:0	85:14:1:0:0	86:13:1:0:0	80:19:1:0:0

All equilibrium fractions $F_0:F_1:F_2:F_3:F_4$ are given in percent. Above the distributions, the equilibrium thicknesses are given in parantheses in units of mg/cm^2. Fractions of less than 0.5% are denoted by 0. In some cases the sum of all fractions is less than 100%, either due to rounding errors or due to the occurence of more than five charge states.

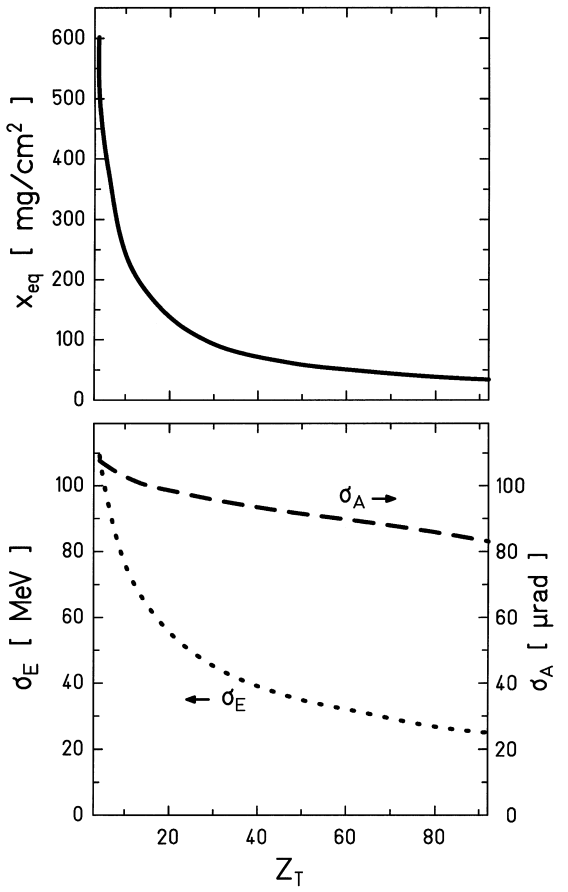

Fig. 16. Upper part: Equilibrium thickness for 4.25-GeV/u Pb ions in different stripper materials Z_T (solid line). Lower part: Energy-loss straggling σ_E (dotted curve, left axis) and multiple scattering σ_A (dashed curve, right axis) of 4.25-GeV/u Pb ions in stripper targets with the equilibrium thickness as displayed in the upper part.

References

[1] N.O. Lassen, Kgl. Dan. Mat. Fys. Medd. 26 (5 and 12) (1951).
[2] N. Bohr, Kgl. Dan. Mat. Fys. Medd. 18 (8) (1948).
[3] N. Bohr, J. Lindhard, Dan. Mat. Fys. Medd. 28 (7) (1954).
[4] H.-D. Betz, Rev. Mod. Phys. 44 (1972) 465.
[5] S.K. Allison, Rev. Mod. Phys. 30 (1958) 1137.
[6] P. Sigmund, Nucl. Instr. Meth. B 69 (1992) 113.
[7] S. Datz, H.O. Lutz, L.B. Bridwell, C.D. Moak, H.D. Betz, L.D. Ellsworth, Phys. Rev. A 2 (1970) 430.
[8] W. Erb, GSI-Report GSI-P-7-78, 1978.
[9] B. Franzke, private communication, 1997.
[10] P.H. Mokler, Th. Stöhlker, Adv. At. Mol. Opt. Phys. 37 (1996) 297.
[11] R. Anholt, S.A. Andriamonje, E. Morenzoni, Ch. Stoller, J.D. Molitoris, W.E. Meyerhof, H. Bowman, J.-S. Xu, Z.-Z. Xu, J.O. Rasmussen, D.H.H. Hoffmann, Phys. Rev. Lett. 53 (1984) 234.
[12] Th. Stöhlker, P.H. Mokler, H. Geissel, E.M. Bernstein, C.L. Cocke, C. Kozhuharov, R. Moshammer, G. Münzenberg, F. Nickel, P. Rymuza, C. Scheidenberger, Z. Stachura, J. Ullrich, A. Warczak, Radiat. Eff. Def. 126 (1993) 319.
[13] Th. Stöhlker, H. Geissel, H. Irnich, T. Kandler, C. Kozhuharov, P.H. Mokler, G. Münzenberg, F. Nickel, C. Scheidenberger, T. Suzuki, M. Kucharski, A. Warczak, P. Rymuza, Z. Stachura, A. Kriessbach, D. Dauvergne, B. Dunford, J. Eichler, A. Ichihara, T. Shirai, Phys. Rev. Lett. 73 (1994) 3520.
[14] Th. Stöhlker, P.H. Mokler, C. Kozhuharov, A. Warczak, Comments At. Mol. Phys. 33 (1997) 271.
[15] R. Anholt, Phys. Rev. A 31 (1985) 3579.
[16] W.E. Meyerhof, R. Anholt, J. Eichler, H. Gould, Ch. Munger, J. Alonso, P. Thieberger, H.E. Wegner, Phys. Rev. A 32 (1985) 3291.
[17] R. Anholt, W.E. Meyerhof, H. Gould, Ch. Munger, J. Alonso, P. Thieberger, H.E. Wegner, Phys. Rev. A 32 (1985) 3302.
[18] R. Anholt, W.E. Meyerhof, Phys. Rev. A 33 (1986) 1556.

[19] R. Anholt, Ch. Stoller, J.D. Molitoris, E. Morenzoni, S.A. Andriamonje, W.E. Meyerhof, H. Bowman, J.-S. Xu, Z.-Z. Xu, J.O. Rasmussen, D.H.H. Hoffmann, Phys. Rev. A 33 (1986) 2270.
[20] R. Anholt, U. Becker, Phys. Rev. A 36 (1987) 4628.
[21] Th. Stöhlker, H. Geissel, H. Folger, C. Kozhuharov, P.H. Mokler, G. Münzenberg, D. Schardt, Th. Schwab, M. Steiner, H. Stelzer, K. Sümmerer, Nucl. Instr. Meth. B 61 (1991) 408.
[22] C. Scheidenberger, H. Geissel, Th. Stöhlker, H. Folger, H. Irnich, C. Kozhuharov, A. Magel, P.H. Mokler, R. Moshammer, G. Münzenberg, F. Nickel, M. Pfützner, P. Rymuza, W. Schwab, J. Ullrich, B. Voss, Nucl. Instr. Meth. B 90 (1994) 36.
[23] Th. Stöhlker, C. Kozhuharov, P.H. Mokler, A. Warczak, F. Bosch, H. Geissel, R. Moshammer, C. Scheidenberger, J. Eichler, A. Ichihara, T. Shirai, Z. Stachura, P. Rymuza, Phys. Rev. A 51 (1995) 2098.
[24] Th. Stöhlker, D.C. Ionescu, P. Rymuza, F. Bosch, H. Geissel, C. Kozhuharov, T. Ludziejewski, P.H. Mokler, C. Scheidenberger, Z. Stachura, A. Warczak, R.W. Dunford, Phys. Rev. A 57 (1998) 845.
[25] Th. Stöhlker, T. Ludziejewski, H. Reich, K. Beckert, F. Bosch, R.W. Dunford, B. Franzke, C. Kozhuharov, G. Menzel, P.H. Mokler, F. Nolden, H.T. Prinz, P. Rymuza, Z. Stachura, M. Steck, P. Swiat, A. Warczak, T. Winkler Phys. Rev. A, to be published.
[26] R. Anholt, W.E. Meyerhof, X.-Y. Xu, H. Gould, B. Feinberg, R.J. McDonald, H.E. Wegner, P. Thieberger, Phys. Rev. A 36 (1987) 1586.
[27] P. Rymuza, Th. Stöhlker, C.L. Cocke, H. Geissel, C. Kozhuharov, P.H. Mokler, R. Moshammer, F. Nickel, C. Scheidenberger, Z. Stachura, J. Ullrich, A. Warczak, J. Phys. B 26 (1993) L169.
[28] Th. Stöhlker, D.C. Ionescu, P. Rymuza, T. Ludziejewski, P.H. Mokler, H. Geissel, C. Scheidenberger, F. Bosch, B. Franzke, O. Klepper, C. Kozhuharov, R. Moshammer, F. Nickel, H. Reich, Z. Stachura, A. Warczak, Nucl. Instr. Meth. B 124 (1997) 160.
[29] R. Anholt, Phys. Rev. A 19 (1979) 1004.
[30] N. Claytor, A. Belkacem, T. Dinneen, B. Feinberg, H. Gould, Phys. Rev. A 55 (1997) R842.
[31] H.F. Krause, C.R. Vane, S. Datz, P. Grafström, H. Knudsen, C. Scheidenberger, R.H. Schuch, Phys. Rev. Lett. 80 (1998) 1190.
[32] J. Eichler, W.E. Meyerhof, Relativistic Atomic Collisions, Academic Press, New York, 1995. (Part of Section 3 is taken from Section 11.2 of this book by permission of the publisher).
[33] M. Stobbe, Ann. Phys. 7 (1930) 601.
[34] H.A. Bethe, E.E. Salpeter, Quantum Mechanics of One- and Two-Electron Atoms, Plenum Press, New York, 1977.
[35] A. Ichihara, T. Shirai, J. Eichler, Phys. Rev. A 49 (1994) 1875.
[36] J. Eichler, Phys. Rev. A 32 (1985) 112.
[37] T. Kandler, P.H. Mokler, Th. Stöhlker, H. Geissel, H. Irnich, Ch. Kozhuharov, A. Kriessbach, M. Kucharski, G. Münzenberg, F. Nickel, P. Rymuza, C. Scheidenberger, Z. Stachura, T. Suzuki, A. Warczak, D. Dauvergne, R.W. Dunford, Phys. Lett. A 204 (1995) 274.
[38] P. Sigmund, in: A. Gras-Marti et al. (Eds.), Interaction of Charged Particles with Solids and Surfaces, NATO ASI Series B, vol. 271, Plenum Press, New York, 1991, p. 73.
[39] P. Sigmund, Phys. Rev. A 50 (1994) 3197.
[40] H.D. Betz, R. Höppler, R. Schramm, W. Oswald, Nucl. Instr. Meth. B 33 (1988) 185.
[41] J.P. Rozet, C. Stephan, D. Vernhet, Nucl. Instr. Meth. B 107 (1996) 67.
[42] H.D. Betz, L. Grodzins, Phys. Rev. Lett. 25 (1970) 903.
[43] W.E. Meyerhof, R. Anholt, X.-Y. Xu, Phys. Rev. A 35 (1987) 1055.
[44] P. Thieberger, H.E. Wegner, J. Alonso, H. Gould, C. Munger, R. Anholt, W.E. Meyerhof, IEEE Trans. Nucl. Sci. 32 (1985) 1767.
[45] H.D. Betz, in: S. Datz (Ed.), Applied Atomic Collision Physics, vol. 4, Academic Press, New York, 1983, p. 2.
[46] CHARGE: The program CHARGE is available at GSI under UNIX and VMS, and is available in the WWW under http://www.gsi.de/~scheid/charge.html.
[47] J.C. Slater, Phys. Rev. 36 (1930) 571.
[48] GLOBAL: The GLOBAL program is available via anonymous ftp from borsu8.in2p3.fr in the directory /pub/nex/global/pc and /pub/nex/global/vms_unix for PCs and workstations, repectively.
[49] See, e.g., S.E. Koonin, Computational Physics, Benjamin-Cummings, Menlo Park, CA, 1986, p. 29.
[50] T.A. Carlson, C.W. Nestor, Jr., N. Wasserman, J.D. McDowell, Atomic Data 2 (1970) 63.
[51] H. Haseroth, in: Proceedings of the Fourth European Particle Accelerator Conference'94, 1994, p. 128.
[52] J. Lindhard, A.H. Sørensen, Phys. Rev. A 53 (1996) 2443.
[53] G. Arduini, R. Bailey, T. Bohl, H. Burkhardt, R. Cappi, C. Carter, K. Cornelis, M. Dach, G. de Rijk, A. Faugier, G. Ferioli, H. Jakob, M. Jonker, D. Manglunki, G. Martini, M. Martini, J.P. Riunaud, C. Scheidenberger, B. Vandorpe, L. Vos, M. Zanolli, in: Proceedings of the Fifth European Particle Accelerator Conference'96, 1996, p. 380.